Atmospheric Chemistry of CH_2BrCl: Kinetics and Mechanism of the Reaction of F Atoms with CH_2BrCl and Fate of the $CHBrClO^{\bullet}$ Radical

Merete Bilde,[†] Jens Sehested,*[,‡] and Ole John Nielsen*[,§]

Section for Chemical Reactivity, Environmental Science and Technology Department, Risø National Laboratory, DK-4000 Roskilde, Denmark

Timothy J. Wallington*[,∥]

Ford Motor Company, Ford Research Laboratory, P.O. Box 2053, SRL-3083, Dearborn, Michigan 48121-2053

Received: February 11, 1997; In Final Form: April 8, 1997[⊗]

The reaction of F atoms with CH_2BrCl was studied using a pulsed radiolysis technique and found to proceed via two channels: direct hydrogen abstraction and adduct formation. The adduct exists in equilibrium with F atoms and CH_2BrCl. The equilibrium constant K_4 = [Adduct]/([CH_2BrCl][F]) = $(4.2 \pm 1.0) \times 10^{-16}$ cm^3molecule^{-1}. In 1000 mbar total pressure of SF_6 at 294 ± 2 K, the yield of the adduct is 68 ± 11% and the overall rate constant for reaction of F atoms with CH_2BrCl is k_4 (1000 mbar) = $(3.6 \pm 0.9) \times 10^{-11}$ cm^3 molecule^{-1} s^{-1}. The adduct reacts with NO with a rate constant of $(2.09 \pm 0.41) \times 10^{-11}$ cm^3 molecule^{-1} s^{-1}. The atmospheric fate of the alkoxy radical CHBrClO is Br atom elimination, which occurs at a rate estimated to be $>2 \times 10^6$ s^{-1} in 700 Torr of air at 295 K. Relative rate techniques were used to measure $k(Cl + CH_2BrCl) = (4.2 \pm 0.5) \times 10^{-13}$ and $k(F + CH_2BrCl \rightarrow CHBrCl + HF) = (1.2 \pm 0.4) \times 10^{-11}$ cm^3 molecule^{-1} s^{-1}. These results are compared to the available literature data.

1. Introduction

The use of bromine-containing organic compounds as fire-extinguishing agents (e.g., CF_3Br and CF_2ClBr) and as soil fumigants (e.g., methyl bromide) is subject to increasing concern because of their adverse impact on stratospheric ozone.[1] CH_2BrCl is a potential substitute for CF_3Br (Halon 1301) and CF_2ClBr (Halon 1211) in certain fire-fighting applications. Interestingly, CH_2BrCl was used as a fire suppression agent by the German Luftwaffe in World War II.[2]

It has recently been shown[3] that the atmospheric life time of CH_2BrCl is largely determined by reaction with OH radicals. By analogy to other hydrogen-containing species[4] reaction of CH_2BrCl with OH radicals produces a halogenated alkyl radical which will, in turn, react with O_2 to give a peroxy radical:

$$CH_2BrCl + OH \rightarrow CHBrCl + H_2O \quad (1)$$

$$CHBrCl + O_2 + M \rightarrow CHBrClO_2 + M \quad (2)$$

In the atmosphere the peroxy radical $CHBrClO_2$ will react with NO and be converted into the corresponding alkoxy radical CHBrClO. As part of a joint program between our two laboratories to survey the atmospheric fate of brominated methanes,[5,6] we have conducted an experimental study of the atmospheric chemistry of CH_2BrCl. A pulse radiolysis technique was used to determine the kinetics and mechanism of the reaction of F atoms with CH_2BrCl. In this work we show that the reaction of F atoms with CH_2BrCl proceeds via two reaction channels: formation of an adduct and direct hydrogen abstraction. The formation of adducts from the reaction of F atoms with other brominated methanes has been reported in recent work from our laboratory,[5,6] and we will compare kinetics and UV absorption data for these different adducts. The formation of a short-lived molecular complex from the reaction of Cl atoms with CH_3I and CH_3Br has been reported by Wine et al.[7]

The atmospheric fate of CHBrClO radicals was determined using a FTIR spectrometer coupled to an atmospheric reactor. Results are reported herein.

2. Experimental Section

Two experimental systems were used; both have been described in detail previously[8,9] and are discussed briefly here.

2.1. Pulse Radiolysis System. Reactions were initiated by the irradiation of SF_6/CH_2BrCl, $SF_6/CH_2BrCl/CH_4$, and $SF_6/CH_2BrCl/NO$ mixtures in a 1 L stainless steel reaction cell with a 30 ns pulse of 2 MeV electrons from a Febetron 705B field emission accelerator. SF_6 was always in great excess and was used to generate fluorine atoms:

$$SF_6 \xrightarrow{2\ \text{MeV}\ e^-} F + \text{products} \quad (3)$$

The total pressure was varied over the range 52−1000 mbar. The radiolysis dose was varied by insertion of stainless steel attenuators between the accelerator and the chemical reactor. We will refer to the radiolysis dose used in specific experiments as a fraction of the maximum dose that is achievable. The fluorine atom yield (required for quantification of UV absorption spectra) was determined by monitoring the transient absorption at 260 nm due to CH_3O_2 radicals produced by radiolysis of $SF_6/CH_4/O_2$ mixtures. Using $\sigma(CH_3O_2) = 3.18 \times 10^{-18}$ cm^2 molecule^{-1}, [10] the F atom yield was calculated to be $[F]_0 = (3.18 \pm 0.32) \times 10^{15}$ molecules cm^{-3} at full radiolysis dose and 1000 mbar of SF_6.[11] Uncertainties reported in this paper are two standard deviations unless otherwise stated. Standard error propagation methods were used to calculate combined uncertainties.

* To whom correspondence should be addressed.
[†] Email: merete.bilde@risoe.dk.
[‡] Email: ker-jese@risoe.dk.
[§] Email: ojn@risoe.dk.
[∥] Email: twalling@ford.com.
[⊗] Abstract published in *Advance ACS Abstracts,* June 1, 1997.

S1089-5639(97)00530-6 CCC: $14.00

Transient absorptions were followed by multipassing the output of a pulsed 150 Watt Xenon arc lamp through the reaction cell using internal White cell optics. Total optical path lengths of 80 and 120 cm were used. After leaving the cell, the light was guided through a 1 m McPherson grating UV−vis monochromator and detected with a Hamamatsu photomultiplier. The spectral resolution was 0.8 nm. Typically, absorption transients were produced in single-pulse experiments with no signal averaging. A Princeton Applied Research OMA-II diode array was used to measure UV absorption spectra. The diode array was installed at the exit slit of the monochromator in place of the photomultiplier which was used for measuring transient absorptions.

Reagent concentrations used were SF_6, 47−1000 mbar; CH_2BrCl, 0.1−20 mbar; CH_4, 0−20.2 mbar; and NO, 0−5 mbar. All experiments were performed at 294 K. SF_6 (99.9%) and CH_4 (>99%) were supplied by Gerling and Holz, CH_2BrCl (>99%) was supplied by Aldrich Chemical Co., Ltd. All gaseous reagents were used as received. CH_2BrCl is a liquid at room temperature and was degassed through several freeze−pump−thaw cycles before use. Partial pressures of the different gases were measured with a Baratron absolute membrane manometer with a detection limit of 10^{-5} bar.

2.2. FTIR−Smog Chamber System. The FTIR system was interfaced to a 140 L Pyrex reactor.[9] Radicals were generated by the UV irradiation of mixtures of 3−30 mTorr of CH_2BrCl, 176−295 mTorr of Cl_2, 0−14 mTorr of NO, and 7−700 Torr of O_2 with N_2 added where appropriate to give a total pressure of 700 Torr. The loss of reactants and the formation of products were monitored by FTIR spectroscopy, using an analyzing path length of 27 m and a resolution of 0.25 cm^{-1}. Infrared spectra were derived from 32 coadded interferograms. CH_2BrCl, HC(O)Cl, and CO were monitored using their characteristic features over the wave number range 700−2000 cm^{-1}. With the exception of HC(O)Cl, reference spectra were acquired by expanding known volumes of reference materials into the chamber. HC(O)Cl was identified by means of its characteristic IR features at 1305 and 1784 cm^{-1} and was quantified using $\sigma(1793\ cm^{-1}) = 1.63 \times 10^{-18}\ cm^2\ molecule^{-1}$ at 295 K.[12]

3. Results and Discussion

3.1. Reaction of F atoms with CH_2BrCl. Figure 1 shows the UV absorption spectrum observed 1−3 μs after the pulse radiolysis of a mixture of 5 mbar of CH_2BrCl and 995 mbar of SF_6. The UV path length was 80 cm, the spectral resolution was 2.24 nm, and the radiolysis dose was 42% of maximum. The spectrum is an average of three spectra obtained under similar conditions and shows two absorption maxima, one centered around 255 nm and the other around 300 nm. The form of this spectrum is similar to those of products formed in the reaction of F atoms with CF_2BrH[5] and CH_3Br.[6] By analogy to the reactions of F atoms with CF_2BrH and CH_3Br, we expect that the reaction of fluorine atoms with CH_2BrCl proceeds via two channels: adduct formation, reaction 4a; and hydrogen abstraction, reaction 4b:

$$CH_2BrCl + F \rightleftharpoons CH_2BrCl\cdots F \qquad (4a, -4a)$$

$$CH_2BrCl + F \rightarrow CHBrCl + HF \qquad (4b)$$

By analogy to the CF_2BrH and the CH_3Br systems, we ascribe the absorption band at 300 nm to the $CH_2BrCl\cdots F$ adduct and that centered at 255 nm to a sum of contributions from the CHBrCl radical and the $CH_2BrCl\cdots F$ adduct. CH_2Br, CH_2Cl, and $CHCl_2$ radicals display maximum UV absorbance at approximately 230,[13] 200,[14] and 215 nm,[14] respectively, and do not absorb appreciably at wavelengths >270 nm. On the basis of these results, it seems very unlikely that the CHBrCl radical absorbs significantly at 310 nm. In the rest of this paper we rely on the assumption that only the adduct absorbs at 310 nm.

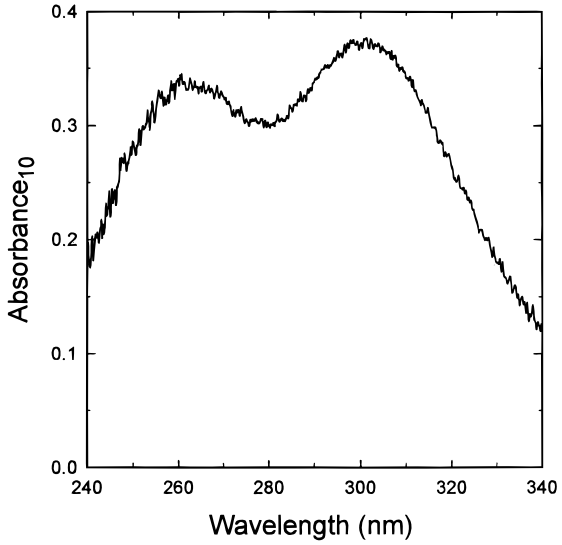

Figure 1. UV absorption spectrum recorded 1−3 μs after the electron pulse following radiolysis of a mixture of 5 mbar of CH_2BrCl and 995 mbar of SF_6. The UV pathlength was 80 cm and the radiolysis was 42% of maximum.

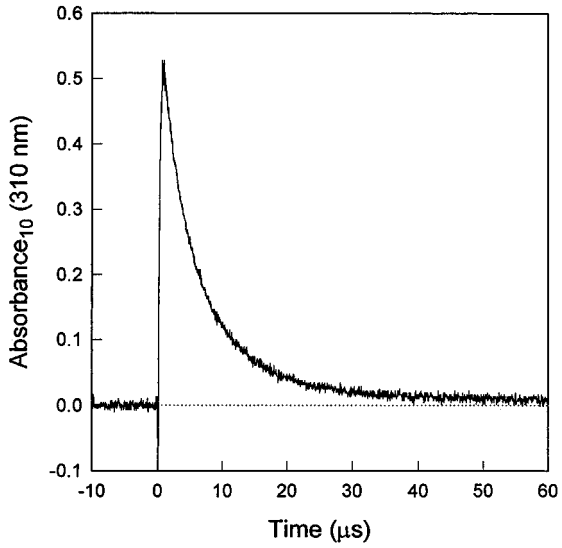

Figure 2. Transient absorbance at 310 nm following the pulsed radiolysis (32% of maximum dose) of 5 mbar of CH_2BrCl and 995 mbar of SF_6. The UV path length was 120 cm.

3.2. Determination of the Equilibrium Constant. To investigate the equilibrium constant $K_4 = k_{4a}/k_{-4a}$, five sets of experiments were performed in which the maximum absorbance at 310 nm following pulsed radiolysis of CH_2BrCl/SF_6 mixtures was measured. In each set of experiments the initial concentrations of CH_2BrCl and SF_6 were constant and only the radiolysis dose was varied. Five initial concentrations of CH_2BrCl were used: 0.1, 0.25, 1.0, 2.0, and 5.0 mbar. Figure 2 shows an example of a transient absorption obtained with a mixture containing 5 mbar of CH_2BrCl. Figure 3 shows plots of the maximum absorbances as functions of the radiolysis dose for different initial concentrations of CH_2BrCl. Although some of the plots are slightly curved it is clear that the maximum absorbance depends on the initial concentration of CH_2BrCl. If the reaction of F atoms with CH_2BrCl proceeded only via

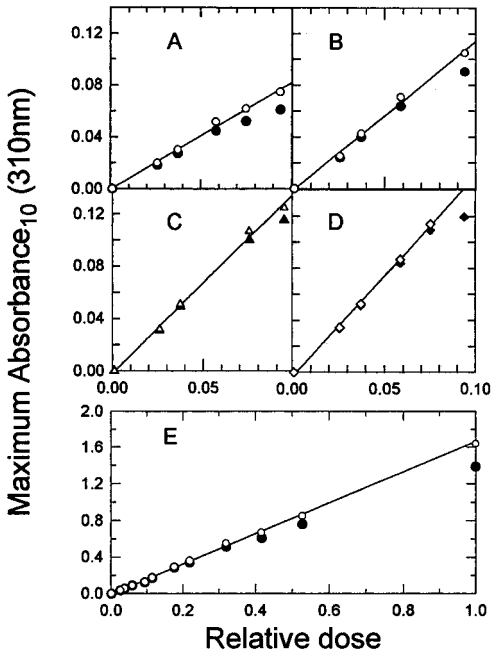

Figure 3. Maximum transient absorbances at 310 nm following the pulsed radiolysis of mixtures of (A) 0.1 mbar CH_2BrCl, (B) 0.25 mbar CH_2BrCl, (C) 1 mbar CH_2BrCl, (D) 2 mbar CH_2BrCl, and (E) 5 mbar CH_2BrCl, all in 1000 mbar total pressure of SF_6, as a function of the radiolysis dose. The UV path length was 120 cm in all experiments. Solid symbols are the observed data; open symbols have been corrected for the influence of reaction 6. The solid lines are linear regressions to the corrected data.

hydrogen abstraction, then the absorbance derived from the low-dose data should be independent of the initial concentration of CH_2BrCl. This is not the case. The dependence of the observed absorption at 310 nm on the CH_2BrCl concentration is consistent with the formation of an adduct which exists in dynamic equilibrium with F atoms and CH_2BrCl

$$CH_2BrCl + F \rightleftharpoons X \rightarrow P \qquad (4a, -4a, 6)$$

$$CH_2BrCl + F \rightarrow CHBrCl + HF \qquad (4b)$$

where "X" is the $CH_2BrCl\cdots F$ adduct and reaction 6 represents the reaction of the adduct with other radicals as discussed in section 3.6. In the Appendix it is shown that the maximum concentration of the $CH_2BrCl\cdots F$ adduct $[X]_{max}$ can be expressed as an analytical function of k_{4a}, k_{-4a}, k_{4b}, and k_6. Initial estimates of $k_{-4a}/k_{4a} = 2.88 \times 10^{15}$ cm^{-1}molecule and $k_{4b}/k_{4a} = 0.42$ were obtained from a fit of equation XII in the appendix to the observed data in Figure 3. The maximum concentration of adduct was calculated for each dose and concentration of CH_2BrCl in the experiments using expression XI in the appendix with (i) k_6 calculated using k_6 = dose (3.88×10^5 s^{-1}) from section 3.6 and (ii) $k_6 = 0$. To obtain the maximum absorbance in the absence of reaction 6, each observed data point in Figure 3 was multiplied by the correction factor $1 + ([X]_{max}^{i} - [X]_{max}^{ii})/[X]_{max}^{ii}$. The open symbols in Figure 3 represent data corrected for k_6, that is, they show the maximum absorbance as it would be if the adduct did not react with other radicals but only decomposed to reform F atoms and CH_2BrCl. The solid lines are linear least-squares fits to the corrected data. The slopes of the linear regressions were 0.82 ± 0.06, 1.15 ± 0.10, 1.38 ± 0.10, 1.55 ± 0.08, and 1.67 ± 0.01 for initial concentrations of 0.1, 0.25, 1.0, 2.0, and 5.0 mbar of CH_2BrCl, respectively. (Due to the high absorbances we only used data up to dose 0.22 for $[CH_2BrCl] = 5$ mbar). From the low-dose data using 5 mbar of CH_2BrCl (Figure 3E) we can calculate

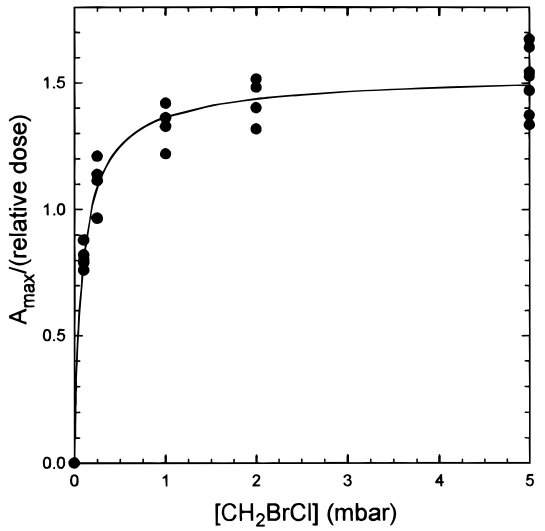

Figure 4. Plot of normalized maximum transient absorbance at 310 nm as a function of $[CH_2BrCl]$. The UV path length was 120 cm. See text for details.

the absorption cross section of the adduct at 310 nm. We assume that for a concentration of 5 mbar CH_2BrCl the equilibrium is shifted totally toward the right and that the maximum concentration of adduct is close to $[F]_0 k_{4a}/(k_{4a} + k_{4b})$. In section 3.5 it will be shown that at 1000 mbar total pressure of SF_6 the fraction of F atoms that forms an adduct, $k_{4a}/(k_{4a} + k_{4b})$, is 0.68 ± 0.11. Using $k_{4a}/(k_{4a} + k_{4b}) = 0.68 \pm 0.11$ and two additional pieces of information: (i) the initial concentration of fluorine atoms using full radiolysis dose of $[F]_0 = (3.18 \pm 0.32) \times 10^{15}$ molecules cm^{-3} and (ii) the maximum absorbance of 1.67 ± 0.01, we are able to calculate the absorption cross section of the adduct at 310 nm, $\sigma_X^{310\ nm} = 1.67\ \ln 10/(0.68[F]_0 120\ cm) = (1.48 \pm 0.28) \times 10^{-17}$ cm^2 molecule^{-1}.

In Figure 4 the absorbances obtained from linear least-squares analysis of the corrected data in Figure 3 are plotted against the concentration of CH_2BrCl. Since the corrected data represent a system with $k_6 = 0$, $[X]_{max}$ is given by (see the Appendix for further details).

$$[X]_{max} = \frac{[CH_2BrCl][F]_0}{n_1 - n_2}\left(\left(\frac{n_1}{n_2}\right)^{n_1/(n_2-n_1)} - \left(\frac{n_1}{n_2}\right)^{n_2/(n_2-n_1)}\right) \qquad (I)$$

where

$$n_1 = \frac{-(1+\alpha)[RH] - k + \sqrt{((1+\alpha)[RH] + k)^2 - 4k\alpha[RH]}}{2}$$

$$n_2 = \frac{-(1+\alpha)[RH] - k - \sqrt{((1+\alpha)[RH] + k)^2 - 4k\alpha[RH]}}{2}$$

The equilibrium constant can be determined from a two parameter fit of the expression $A_{max} = \sigma_X^{310\ nm} 120\ cm([X]_{max}/\ln 10)$ to the data in Figure 4 where $[X]_{max}$ is defined by the equation given above (equation XII in the Appendix). The best fit is shown as the smooth curve in Figure 4 and was obtained using $k = k_{-4a}/k_{4a} = (2.38 \pm 0.06) \times 10^{15}$ and $\alpha = k_{4b}/k_{4a} = (0.60 \pm 0.06)$. The equilibrium constant is $K_4 = 1/k = (4.20 \pm 1.01) \times 10^{-16}$ cm^3 molecule^{-1}.

3.3. Determination of $k(F + CH_2BrCl)$ Relative to $k(F + CH_4)$ Using the Pulsed Radiolysis System. To confirm that

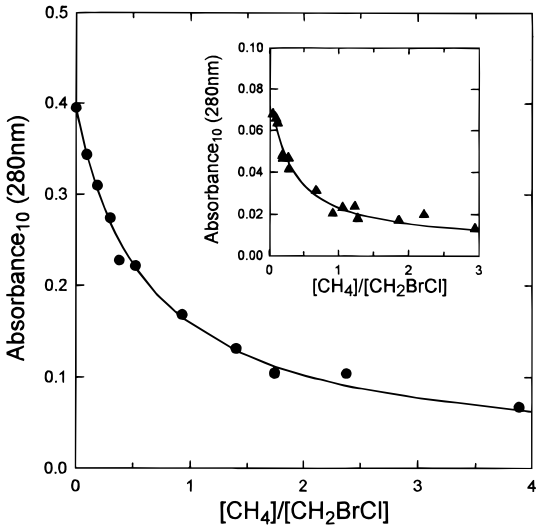

Figure 5. Plot of maximum absorption at 280 nm versus the concentration ratio $[CH_4]/[CH_2BrCl]$. Circles, 1000 mbar total pressure of SF_6. Triangles, 200 mbar total pressure of SF_6. See text for details.

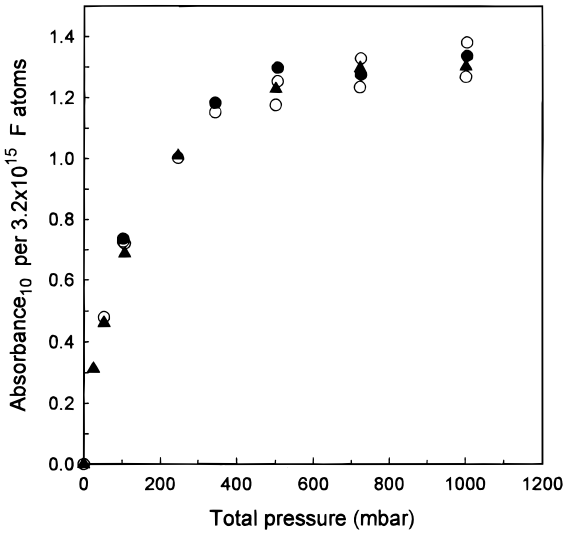

Figure 6. Plot of maximum absorption per 3.18×10^{15} F atoms versus total pressure. The UV path length was 120 cm. Full radiolysis dose. $[CH_2BrCl] = 5$ mbar, $[SF_6] = 0-1000$ mbar. Circles, full radiolysis dose; triangles, 52% of maximum dose. Solid symbols represent observed data; open symbols represent simulated data. See text for details.

the specie(s) responsible for the observed absorption at 280 nm is (are) indeed formed from the reaction of F atoms with CH_2BrCl, a set of experiments was performed with CH_4 added to provide an additional loss mechanism for F atoms:

$$F + CH_4 \rightarrow CH_3 + HF \qquad (5)$$

In these experiments the concentration of CH_2BrCl was kept constant at 5 mbar, the concentration of CH_4 was varied over the range 0−20.2 mbar, and SF_6 was added to give a total pressure of 1000 mbar. In all experiments, the radiolysis dose was 32% of maximum, the optical path length was 120 cm, and the maximum transient absorption was measured. Figure 5 shows the observed maximum absorbance as a function of the concentration ratio $[CH_4]/[CH_2BrCl]$. As seen from Figure 5, the addition of CH_4 results in a decrease in the observed maximum transient absorption at 280 nm. The reaction of F atoms with CH_4 is rapid, $k_5 = 6.8 \times 10^{-11}$ cm^3 molecule^{-1} s^{-1}.[15] CH_4 is an efficient scavenger of F atoms. In contrast, we do not anticipate that CH_4 is an efficient scavenger of other radicals potentially formed in the system. The fate of CH_3 radicals in the chamber is self-reaction, reaction with CHBrCl, or reaction with $CH_2BrCl\cdots F$. If the species responsible for the absorption at 280 nm observed in the SF_6/CH_2BrCl experiments was not formed from the reaction of F atoms with CH_2BrCl, the observed absorbance should be independent of the partial pressure of CH_4. The fact that this is not the case suggests strongly that the radicals responsible for the absorption at 280 nm are formed by reaction of F atoms with CH_2BrCl.

The competition between reactions 4 and 5 was used to determine the rate constant for reaction 4. The solid line in Figure 5 represents a three-parameter fit of the expression below to the experimental data:

$$A_{max} = \frac{A_{F+CH_2BrCl} + A_{F+CH_4}\frac{k_5}{k_4}\frac{[CH_4]}{[CH_2BrCl]}}{1 + \frac{k_5}{k_4}\frac{[CH_4]}{[CH_2BrCl]}} \qquad (II)$$

where A_{max} is the observed maximum absorbance, $A_{F+CH2BrCl}$ is the absorbance in the absence of CH_4, and A_{F+CH_4} is the absorbance in the absence of CH_2BrCl. A_{F+CH_2BrCl}, A_{F+CH_4}, and k_5/k_4 were simultaneously varied and the best fit was achieved with $A_{F+CH_2BrCl} = (0.39 \pm 0.02)$, $A_{F+CH_4} = (0.01 \pm 0.01)$, and $k_5/k_4 = (1.61 \pm 0.28)$. The solid line in Figure 5 shows the fit. A control experiment using a mixture of 40 mbar of CH_4 and 960 mbar of SF_6 confirmed that $A_{F+CH_4} \approx 0$. Using $k_5 = (6.8 \pm 1.4) \times 10^{-11}$,[15,16] gives k_4 (1000 mbar) $= (4.23 \pm 1.13) \times 10^{-11}$ cm^3 molecule^{-1} s^{-1}. The experiment was repeated at 200 mbar total pressure of SF_6 using a dose of 42% of maximum, $[CH_2BrCl] = 5$ mbar, and $[CH_4] = 0-15.3$ mbar. A three-parameter fit to the 200 mbar data gave $A_{F+CH_2BrCl} = (0.08 \pm 0.01)$, $A_{F+CH_4} = (0.005 \pm 0.005)$, and $k_5/k_4 = (3.16 \pm 1.39)$. Using $k_5 = (6.8 \pm 1.4) \times 10^{-11}$,[15] gives k_4 (200 mbar) $= (2.15 \pm 1.04) \times 10^{-11}$ cm^3 molecule^{-1} s^{-1}. The overall rate constant $k_4 = (k_{4a} + k_{4b})$ for the reaction of F atoms with CH_2BrCl decreases substantially as the total pressure is reduced from 1000 to 200 mbar of SF_6. This observation suggests that at 1000 mbar total pressure a substantial fraction of reaction 4 proceeds via channel 4a. A detailed account of the results from a series of experiments to map out the pressure dependence of reaction 4 is presented in section 3.4.

From the FTIR results (section 3.7) we know that $k_5/k_{4b} = (5.3 \pm 0.8)$, and hence, from k_5/k_4(1000 mbar) $= (1.61 \pm 0.28)$ and k_5/k_4 (200 mbar) $= (3.16 \pm 1.39)$ we can calculate the adduct yield $Y_X(M) = (k_4\,(M) - k_{4b})/k_4(M)$ at 1000 mbar and 200 mbar total pressure of SF_6. We obtain Y_X(1000 mbar) $= (0.70 \pm 0.11)$ and Y_X(200 mbar) $= (0.40 \pm 0.28)$. We are also in a position to calculate k_{-4a} from $k_{4a} = k_5(k_4/k_5 - k_{4b}/k_5) = (2.94 \pm 0.95) \times 10^{-11}$ cm^3 molecule^{-1} s^{-1} at 1000 mbar total pressure. Using $K_4 = k_{4a}/k_{-4a} = (4.2 \pm 1.0) \times 10^{-16}$ cm^3 molecule^{-1} from section 3.2, we derive $k_{-4a} = k_{4a}/K_4 = (7.0 \pm 2.8) \times 10^4$ s^{-1} at 1000 mbar total pressure of SF_6.

3.4. Pressure Dependence of the Adduct Formation. A series of experiments was performed to investigate the influence of total pressure on the formation of the adduct. Mixtures of CH_2BrCl/SF_6 were subject to pulsed radiolysis, and the formation of the adduct was detected at 310 nm. The initial concentration of CH_2BrCl was fixed at 5 mbar, the radiolysis dose was 52−100% percent of maximum, and the total pressure of SF_6 was varied over the range 20−1000 mbar. The UV path length in the cell was 120 cm. Figure 6 shows the observed maximum absorbance per 3.18×10^{15} F atoms generated by the radiolysis pulse versus the total pressure. We ascribe the

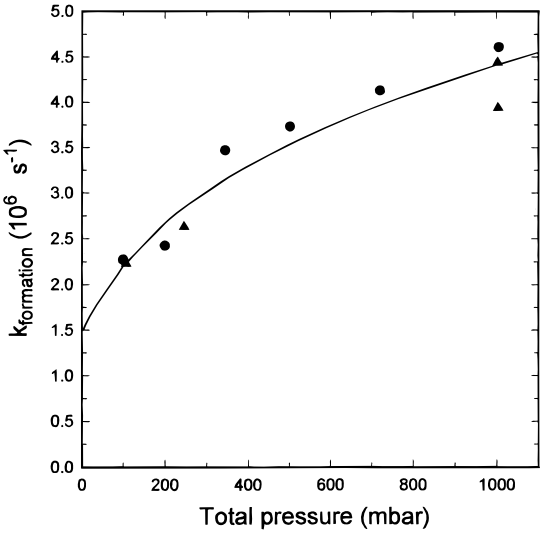

Figure 7. Plot of the formation rate $k_{formation}$ obtained from first-order fits to the experimental transients at 310 nm following radiolysis of mixtures of 5 mbar CH_2BrCl and 100−1000 mbar of SF_6 versus total pressure.

falloff of this curve to a decrease in the formation of the adduct at low pressures.

Mathematically, the falloff can be described by the parametrization proposed by Troe[17] and recommended by the NASA data evaluation committee[18] to describe addition and thermal dissociation reactions in atmospheric models:

$$A([M]) = [X]_{max}\frac{\sigma_x l}{\ln 10}$$

where

$$[X]_{max} = \frac{k_a[RH][F]_0}{m_1 - m_2}\left(\left(\frac{m_1}{m_2}\right)^{m_1/(m_2-m_1)} - \left(\frac{m_1}{m_2}\right)^{m_2/(m_2-m_1)}\right)$$

m_1 and m_2 are given by equation IV in the Appendix, and both terms depend on k_{4a}, $k_{-4a,}$ k_{4b}, and k_6. For k_{4a} the expression below was used

$$k_{4a}([M]) = \frac{k_{4a,0}[M]}{1 + k_{4a,0}[M]/k_{4a,\infty}}\,0.6^{(1+[\log_{10}(k_{4a,0}[M]/k_{4a,\infty})]^2)^{-1}}$$

and for k_{-4a} we used that the equilibrium constant is independent of total pressure and hence $k_{-4a}([M]) = k_{4a}([M])/K_4$ at any given pressure M. We used $K_4 = (4.2 \pm 1.01) \times 10^{-16}$ cm^3 molecule^{-1} determined in section 3.2. $k_{4a,0}$ and $k_{4a,\infty}$ are the limiting low- and high-pressure rate constants for the formation of the adduct, and $A([M])$ is the observed maximum absorbance as a function of the total pressure M. k_6 was calculated separately for each pressure and dose using $k_6 = 3.88 \times 10^5 \times (\text{dose})(p)/1000$ obtained from section 3.6. The expression was fitted to the experimental data in Figure 6 using $\sigma_X^{310nm} = (1.48 \pm 0.28) \times 10^{-17}$ cm^2 molecule^{-1} (determined in section 3.2), an optical path length of $l = 120$ cm, and $k_{4b} = (1.2 \pm 0.4) \times 10^{-11}$ cm^3 molecules^{-1} s^{-1} as obtained from the FTIR experiments (see section 3.7). The best fit was obtained with $k_0 = (1.78 \pm 0.72) \times 10^{-30}$ cm^6 molecule^{-2} s^{-1} and $k_\infty = (8.93 \pm 0.63) \times 10^{-11}$ cm^3 molecules^{-1} s^{-1} and is shown in Figure 6 as open circles. Uncertainties were calculated using standard error propagation methods including uncertainties in $\sigma[F]_0$ and k_{4b}. We can now calculate k_4(M) at 200 and 1000 mbar total pressure of SF_6. We obtain k_4(1000 mbar) = $(3.6 \pm 1.4) \times 10^{-11}$ and k_4(200 mbar) = $(2.1 \pm 0.9) \times 10^{-11}$ cm^3 molecules^{-1} s^{-1}. For k_{-4a}(1000 mbar) we obtain k_{-4a}(1000 mbar) = k_{4a}/K_4 = $(2.40 \pm 0.51) \times 10^{-11}/(4.20 \pm 1.01) \times 10^{-16} = (5.7 \pm 1.8) \times 10^4$ s^{-1} in good agreement with the value of k_{-4a}(1000 mbar) = $(7.0 \pm 2.8) \times 10^4$ s^{-1} obtained in section 3.3. The adduct yields obtained from these rate constants are Y_X(1000 mbar) = (0.67 ± 0.30) and Y_X(200 mbar) = (0.43 ± 0.22).

To confirm these rate constants, a biexponential expression was fitted to the experimental transients. In all cases the transients were well fit by the following biexponential expression:

$$A = A_1 \exp(-k_{form}t_1) + A_2 \exp(-k_{decay}t_2) + A_\infty$$

In Figure 7 pseudo-first-order rate constants $k_{formation}$ for the addition of F atoms to CH_2BrCl are plotted versus the total pressure. As seen from Figure 7 the formation rate increases with increasing total pressure. The expression

$$k_4(M) = k_{4a}(M) + k_{4b}$$

where

$$k_{4a}(M) = \frac{k_{4a,0}[M]}{1 + k_{4a,0}[M]/k_{4a,\infty}}\,0.6^{(1+[\log(k_{4a,0}[M]/k_{4a,\infty})]^2)^{-1}}$$

was used to fit the data. k_{4b} was fixed at the value of $k_{4b} = (1.2 \pm 0.4) \times 10^{-11}$ cm^3 molecules^{-1} s^{-1} obtained from the FTIR experiments (see section 3.7). The best fit was obtained using $k_{4a,0} = (3.51 \pm 2.07) \times 10^{-30}$ cm^6 molecules^{-2} s^{-1} and $k_{4a,\infty} = (7.33 \pm 4.71) \times 10^{-11}$ cm^3 molecules^{-1} s^{-1}. From this we calculate k_4(1000 mbar) = $(3.59 \pm 1.12) \times 10^{-11}$ and k_4(200 mbar) = $(2.17 \pm 0.59) \times 10^{-11}$ cm^3 molecules^{-1} s^{-1}. These results are in excellent agreement with those obtained above and also in good agreement with the values of k_4(1000 mbar) = $(4.23 \pm 1.13) \times 10^{-11}$ and k_4(200 mbar) = $(2.15 \pm 1.04) \times 10^{-11}$ cm^3 molecule^{-1} s^{-1} obtained from the relative rate experiments described in section 3.3. The adduct yields are Y_X(1000 mbar) = (0.67 ± 0.15) and Y_X(200 mbar) = (0.45 ± 0.24).

The results obtained from Figure 6 are based on the assumption that only the adduct absorbs at 310 nm. The results obtained from the pseudo-first-order formation rate constants, Figure 7, are independent of this assumption and so are the numbers obtained from section 3.3 which are also obtained at a different wavelength, namely 280 nm. The results obtained in this section rely on the value of k_{4b} determined in the FTIR experiments, on the other hand the value of k_4 obtained in section 3.3 is independent of the FTIR result. The good agreement between the three sets of results strongly supports the assumption that only the adduct absorbs at 310 nm, and the interpretation of the FTIR experiments to give $k_{4b} = (1.2 \pm 0.4) \times 10^{-11}$ cm^3 molecule^{-1} s^{-1}.

As a final value of k_4, we choose to quote an average of the two values, determined in this section. We arrive at a total rate constant for reaction 4 of $k_4 = (k_{4a} + k_{4b}) = (3.6 \pm 0.9) \times 10^{-11}$ cm^3 molecule^{-1} s^{-1} at 1000 mbar total pressure of SF_6.

3.5. Reaction of the Adduct with NO. To investigate the reaction of the adduct with NO, mixtures of $CH_2BrCl/SF_6/NO$ were subject to pulsed radiolysis and the resulting transient absorption at 310 nm was monitored.

$$CH_2BrCl\cdots F + NO \rightarrow \text{products} \qquad (7)$$

The concentration of CH_2BrCl was kept constant at 5 mbar, the concentration of NO was varied from 0.4 to 2.1 mbar, and

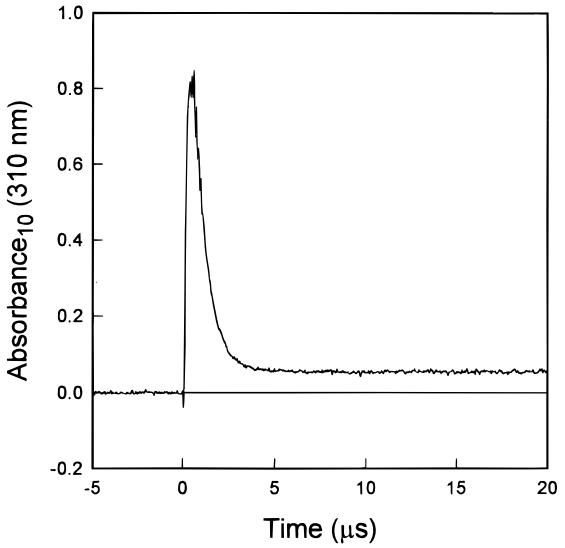

Figure 8. Transient absorbance at 310 nm following the pulsed radiolysis (full dose) of a mixture of 5 mbar CH_2BrCl, 1.8 mbar NO, and 992 mbar SF_6. The UV path length was 120 cm.

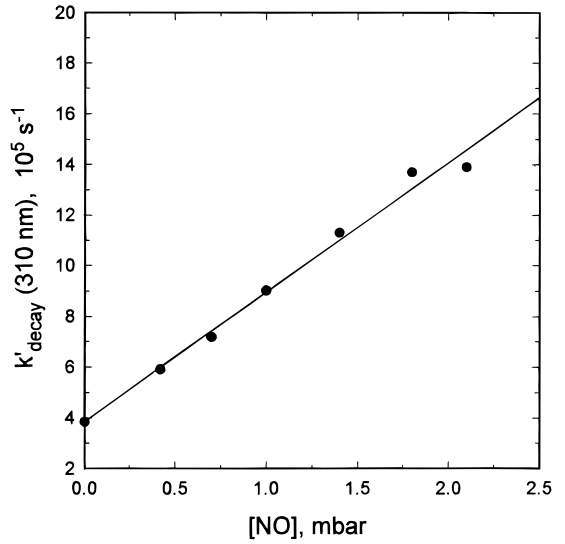

Figure 9. First-order decay rates of the $CH_2BrCl\cdots F$ adduct derived by monitoring the loss of absorption at 310 nm as a function of [NO] following radiolysis of mixtures of 0−2.1 mbar [NO], 5 mbar of CH_2BrCl, and 1000 mbar total pressure of SF_6.

the total pressure was fixed at 1000 mbar. Full radiolysis dose was used, and the optical path length was 120 cm. Figure 8 shows a typical experimental transient. This transient can be compared to the transient obtained in the absence of NO shown in Figure 2. The decay of the adduct is much faster when NO is present. The decays of the observed transients at 310 nm followed first-order kinetics and were fitted using a first-order decay expression ($A = A_1 \exp(-k_7 t) + A_{inf}$) to give pseudo-first-order decay rate constants. Figure 9 shows the pseudo-first-order rate constants for the decay of the adduct versus the concentration of NO. A linear least-squares fit gives $k_7 = (2.09 \pm 0.04) \times 10^{-11}$ cm^3 molecule^{-1} s^{-1}. To take account of potential systematic errors, we chose to add an additional 20% to the uncertainty of k_7. Propagating this additional uncertainty gives $k_7 = (2.09 \pm 0.41) \times 10^{-11}$cm^3 molecule^{-1} s^{-1}. We ascribe the *y*-axis intercept of $(3.84 \pm 0.63) \times 10^5$ s^{-1} to the decay of the adduct in the absence of NO (i.e., the sum of the adduct losses from reactions −4a and 6 and possible self- and cross-reactions.

On the basis of our experience with the CH_3Br--F adduct, it seems likely that the products formed from reaction 7 are FNO

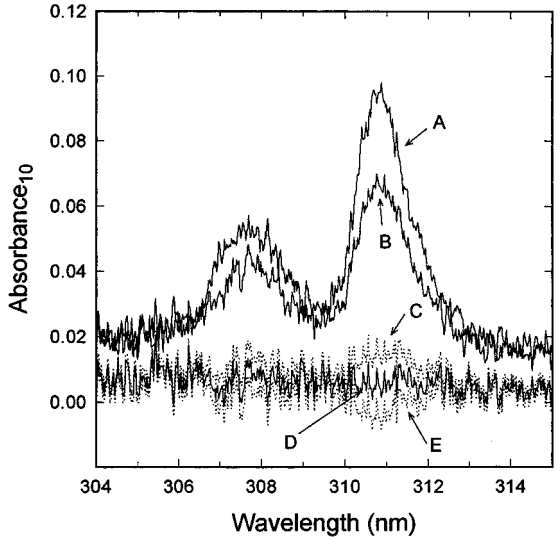

Figure 10. UV absorption spectra obtained 80−83 ms after the electron pulse following radiolysis of spectra A, 5 mbar NO and 995 mbar SF_6 and spectra B 5 mbar NO, 5 mbar CH_2BrCl, and 990 mbar SF_6. Spectra C, D, and E are residual spectra obtained by subtracting 55, 65, and 75% of spectrum A from spectrum B, respectively.

and CH_2BrCl. To test this hypothesis, two chemical systems were subject to pulsed radiolysis: (i) a mixture of 5 mbar NO and 995 mbar SF_6 and (ii) a mixture of 5 mbar CH_2BrCl, 5 mbar NO, and 990 mbar SF_6. UV absorption spectra were recorded over the range 305−316 nm using a resolution of 0.8 nm, a scan time of 3 ms, and full radiolysis dose. In reaction mixture i) the following reactions are important:

$$SF_6 \xrightarrow{2\ \text{MeV e}^-} F + \text{products} \quad (3)$$

$$F + NO + M \rightarrow FNO + M \quad (8)$$

Figure 10, spectrum A, shows the average of three spectra acquired 80−83 ms after radiolysis of reaction mixture (i). The two peaks are well-known FNO features.[19] Figure 10, spectrum B, shows the absorption (average of three spectra) 80−83 ms following radiolysis of reaction mixture (ii). Clearly, FNO is also formed in this system. By making the reasonable assumption that FNO is formed in 100% yield in reaction 7, the adduct yield in reaction 4 is given by the amount of FNO formed in reaction mixture (ii) relative to the amount formed in reaction mixture (i). This ratio was determined by subtraction of spectrum A from spectrum B. In Figure 10 the residual spectra following the subtraction of 55, 65, and 75% of spectrum A from spectrum B are shown. It is evident that the FNO yield in reaction mixture (ii) is 65 ± 10% of that in reaction mixture (i). Two corrections are necessary before a final value for the adduct yield k_{4a}/k_4 can be extracted. First, we have to consider the possible interference from second-order chemistry in the two systems. The maximum absorbance at 310.7 nm following pulsed radiolysis of reaction mixtures (i) and (ii) are plotted versus radiolysis dose in Figure 11. The maximum transient absorbance is proportional to the radiolysis dose over the entire range tested for reaction mixture (i). This is not the case for reaction mixture (ii). The full dose absorbance falls below a linear extrapolation of the low-dose data by a factor of 0.86 ± 0.10. Thus, the amount of FNO actually formed at full dose, relative to the amount of FNO that would have been formed if no secondary chemistry was important, is 0.86. The adduct yield in reaction 4 is then (0.65 ± 0.10)/(0.86 ± 0.10) = (0.76 ± 0.14) at 1000 mbar total pressure of SF_6. Second, correction is needed for direct reaction of F atoms with NO. Using *k*(F +

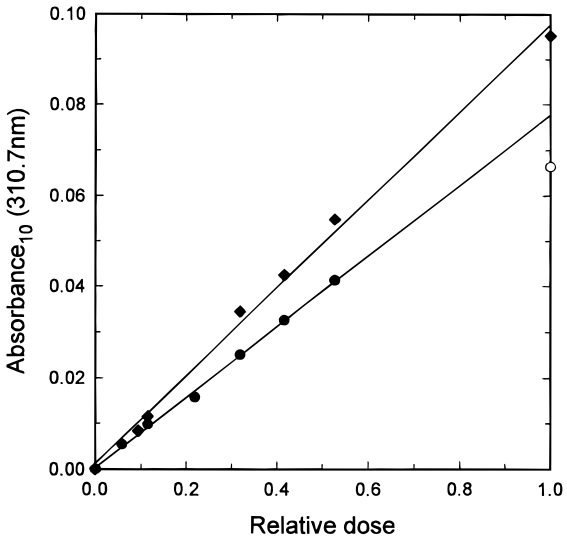

Figure 11. Plot of maximum absorbance at 310.7 nm following radiolysis of mixtures of 5 mbar NO and 995 mbar SF_6 with (circles) or without (diamonds) 5 mbar of added CH_2BrCl.

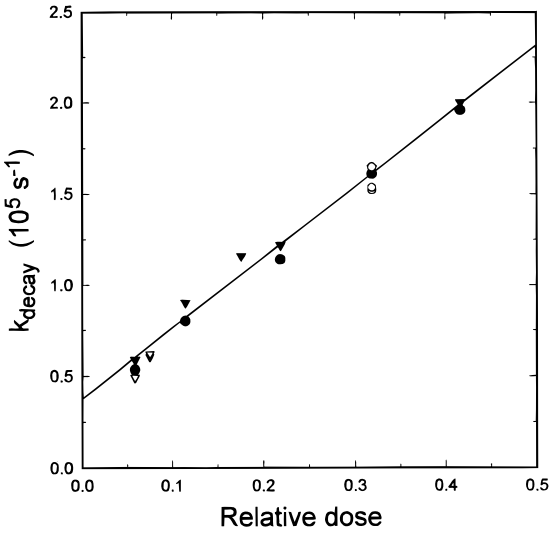

Figure 12. Plot of the first-order decay rate of the adduct versus radiolysis dose following radiolysis of SF_6/CH_2BrCl mixtures. Triangles were obtained using a monitoring wavelength of 310 nm and circles were obtained using 280 nm. See text for details. Closed symbols, $[CH_2BrCl] = 5$ mbar; open symbols, $[CH_2BrCl] = 1-20$ mbar. The straight line is a linear least-squares fit to the 5 mbar data.

NO) $= (5.1 \pm 0.7) \times 10^{-12}$ [20,21] and $k_4 = (3.6 \pm 0.9) \times 10^{-11}$ cm^3 molecule^{-1} s^{-1} we calculate that (12.4 ± 3.6)% of the F atoms react directly with NO in reaction mixture (ii). After applying this final correction the adduct yield is (0.67 ± 0.23). This number is in excellent agreement with the values of (0.70 ± 0.11) obtained in section 3.3 and (0.67 ± 0.15) obtained in section 3.4. While the determinations of k_{4a}/k_4 should strictly be viewed as lower limits, the excellent agreement between the results of the three independent methods suggests that these determinations are close to the true value of k_{4a}/k_4 at 1000 mbar of total pressure. Hence, we choose to report the adduct yield at 1000 mbar total pressure of SF_6 as the average of these three determinations: $Y_{adduct}(1000\ mbar) = 0.68 \pm 0.11$.

3.6. Decay of the Adduct. To investigate the decay of the adduct in the absence of NO, the experimental transients at 280 and 310 nm following radiolysis of 5 mbar CH_2BrCl and 995 mbar SF_6 were fitted using a first-order decay expression which provided a good fit to the experimental data. The radiolysis dose was varied between 6 and 42% of full dose. Figure 12 shows a plot of the first-order decay rate constants as a function of radiolysis dose. There was no discernible difference between results obtained at 280 and 310 nm. The decay rate increased linearly with radiolysis dose suggesting that radical−radical reactions such as reactions 9−12 are important (X≡CH_2BrCl···F):

$$X + X \rightarrow \text{products} \quad (9)$$

$$X + CHBrCl \rightarrow \text{products} \quad (10)$$

$$X + F \rightarrow \text{products} \quad (11)$$

$$X + CH_2BrCl \rightarrow \text{products} \quad (12)$$

A linear least-squares fit to the data in Figure 12 gives a slope of $(3.88 \pm 0.28) \times 10^5$ s^{-1} and an intercept of $(3.75 \pm 0.79) \times 10^4$ s^{-1}. The slope contains information on the kinetics of reactions 9−12 and possibly other reactions. The adduct does not coexist with F atoms ($[X]/[F] = K_4[CH_2BrCl] = 52$), and hence, reaction 11 is unimportant. To investigate the importance of reaction 12 the concentration of CH_2BrCl was varied over the range 1−20 mbar and the pseudo-first-order rate constant for loss of the adduct was measured at 280 nm. Results are shown as hollow symbols in Figure 12. On the basis of these data we conclude that reaction 12 is of minor importance.

Reaction of the adduct with other radicals is represented by reaction 6.

$$CH_2BrCl + F + M \rightleftharpoons X + M \rightarrow \text{products} \quad (4a, -4a, 6)$$

$$CH_2BrCl + F \rightarrow CHBrCl + HF \quad (4b)$$

The intercept contains information concerning the decay k_{-4a}. Decomposition via reaction -4a gives an F atom and one CH_2BrCl molecule. When the F atom reacts again with CH_2BrCl, 68% will reform the adduct and 32% will give the alkyl radical. Therefore we interpret the intercept as $0.32k_{-4a}$. From this we calculate $k_{-4a} < (3.75 \pm 0.79) \times 10^4\ s^{-1}/(0.32 \pm 0.04) = (1.17 \pm 0.29) \times 10^5\ s^{-1}$. This upper limit is consistent with $k_{-4a} = (5.7 \pm 1.8) \times 10^4\ s^{-1}$ obtained in section 3.4 and $k_{-4a} = (7.0 \pm 2.8) \times 10^4\ s^{-1}$ obtained in section 3.3. The adduct may also decompose unimolecularly into products other than F atoms and CH_2BrCl. The intercept provide an upper limit for this reaction of $(3.75 \pm 0.79) \times 10^4\ s^{-1}$.

3.7. Kinetics of the Reactions of Cl and F Atoms with CH_2BrCl. To investigate the kinetics of the reactions of Cl and F atoms with CH_2BrCl, relative rate studies were performed using the FTIR system. The techniques used are described in detail elsewhere.[15,22] Photolysis of molecular chlorine was used as a source of Cl atoms.

$$Cl_2 + h\nu \rightarrow 2Cl \quad (13)$$

The rate of reaction 14 was measured relative to reactions 15 and 16.

$$Cl + CH_2BrCl \rightarrow CHBrCl + HCl \quad (14)$$

$$Cl + CH_4 \rightarrow CH_3 + HCl \quad (15)$$

$$Cl + CH_3Cl \rightarrow CH_2Cl + HCl \quad (16)$$

Figure 13 shows the observed loss of CH_2BrCl versus the losses of the reference compounds following the UV irradiation of mixtures of $CH_2BrCl/CH_4/Cl_2$ and $CH_2BrCl/CH_3Cl/Cl_2$ in 700 Torr of air diluent. Linear least-squares analysis gives $k_{14}/k_{15} = (4.0 \pm 0.3)$ and $k_{14}/k_{16} = (0.88 \pm 0.05)$. Using $k_{15} = 1.0$

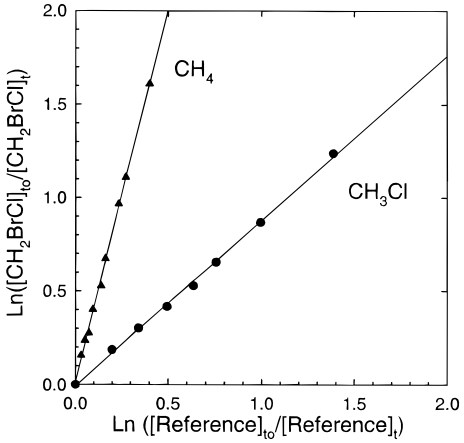

Figure 13. Loss of CH_2BrCl versus CH_4 (triangles) and CH_3Cl (circles) when mixtures containing these compounds were exposed to Cl atoms in 700 Torr of air diluent.

$\times 10^{-13}$ [18] and $k_{16} = 4.9 \times 10^{-13}$ [18] gives $k_{14} = (4.0 \pm 0.3) \times 10^{-13}$ and $k_{14} = (4.3 \pm 0.2) \times 10^{-13}$ cm^3 molecule^{-1} s^{-1}. We choose to quote a final value of $k_{14} = (4.2 \pm 0.5) \times 10^{-13}$ cm^3 molecule^{-1} s^{-1}, which is an average of the two results above with error limits that encompass the extremes of the individual determinations. We estimate that potential systematic errors associated with uncertainties in the reference rate constants could add an additional 10% to the uncertainty range. Propagating this additional 10% uncertainty gives $k_{14} = (4.2 \pm 0.7) \times 10^{-13}$ cm^3 molecule^{-1} s^{-1}. This result is in good agreement with the measurement of $k_{14} = (4.2 \pm 1.2) \times 10^{-13}$ cm^3 molecule^{-1} s^{-1} at 298 K by Tschuikow-Roux et al.[23]

To determine the kinetics of the reaction of F atoms with CH_2BrCl, photolysis of molecular fluorine was used as a source of F atoms. The kinetics of reaction 4 were measured relative to reactions 5, 18, and 19.

$$F_2 + h\nu \rightarrow 2F \quad (17)$$

$$F + CH_2BrCl \rightarrow CHBrCl + HF \quad (4)$$

$$F + CHF_2CH_3\ (HFC\text{-}152a) \rightarrow CHF_2CH_2 + HF \quad (18)$$

$$F + CH_4 \rightarrow CH_3 + HF \quad (5)$$

$$F + CD_4 \rightarrow CD_3 + DF \quad (19)$$

Figure 14 shows the observed losses of CH_2BrCl versus those of the reference compounds following irradiation of mixtures of $CH_2BrCl/CHF_2CH_3/F_2$, $CH_2BrCl/CH_4/F_2$, and $CH_2BrCl/CD_4/F_2$ in 700 Torr of N_2, or air diluent. There was no discernible difference between results obtained in N_2 or air diluent. Linear least-squares analysis gives $k_4/k_{18} = (0.68 \pm 0.05)$, $k_4/k_5 = (0.19 \pm 0.03)$, and $k_4/k_{19} = (0.27 \pm 0.03)$. Using $k_{18} = 1.7 \times 10^{-11}$,[15] $k_5 = 6.8 \times 10^{-11}$,[15,16] and $k_{19} = 4.7 \times 10^{-11}$ [24] gives $k_4 = (1.16 \pm 0.09) \times 10^{-11}$, $k_4 = (1.29 \pm 0.20) \times 10^{-11}$, and $k_4 = (1.26 \pm 0.14) \times 10^{-11}$ cm^3 molecule^{-1} s^{-1}, respectively. We choose to cite a final value for k_4, which is an average of the above values with error limits which encompass the extremes of the determinations, $k_4 = (1.2 \pm 0.3) \times 10^{-11}$ cm^3 molecule^{-1} s^{-1}. We estimate that potential systematic errors associated with uncertainties in the reference rate constants could add an additional 20% to the uncertainty range. Propagating this additional uncertainty gives $k_4 = (1.2 \pm 0.4) \times 10^{-11}$ cm^3 molecule^{-1} s^{-1}.

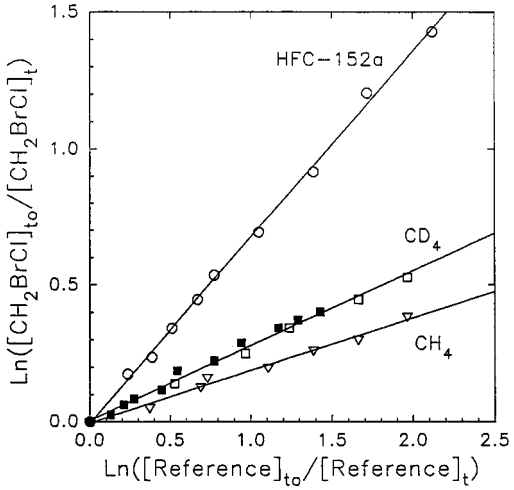

Figure 14. Loss of CH_2BrCl versus CH_3CHF_2 (circles), CD_4 (squares), and CH_4 (triangles) when mixtures containing these compounds were exposed to F atoms in 700 Torr of N_2 (open symbols) or air (filled symbols) diluent.

At this point it is germane to note that the rate constant ratio k_5/k_4 was also studied using the pulsed radiolysis setup (see section 3.3). The result from the FTIR technique in 700 Torr of air diluent was $k_5/k_4 = 5.3 \pm 0.8$ and can be compared directly to the determinations of $k_5/k_4 = (1.61 \pm 0.28)$ and $k_5/k_4 = (3.16 \pm 1.39)$ at 1000 and 200 mbar of SF_6 diluent, respectively, from the pulsed radiolysis experiments. At a first glance it appears that the results obtained using the two different techniques are inconsistent. However, before we compare the results from the two techniques, we must recognize the different time scales and the different radical concentrations of the experiments. The mechanism for the reaction of F atoms with CH_2BrCl is given by reactions 4a, -4a, 6, and 4b.

$$CH_2BrCl + F + M \rightleftharpoons X + M \rightarrow \text{products} \quad (4a, -4a, 6)$$

$$CH_2BrCl + F \rightarrow CHBrCl + HF \quad (4b)$$

Reaction 6 represents loss of the adduct via reaction with other radicals. In the FTIR experiments the F atom concentration is very low ($(2-5) \times 10^6$ molecules cm^{-3}). We know that k_{-4a} is of the order of 7×10^4 s^{-1}. For reaction of the adduct with radical species (reaction 6) to be competitive with decomposition of the adduct (reaction -4a) the pseudo-first-order loss of the adduct via reaction with any radical "Y" must be of the order of 10^5 s^{-1}. If we assume an upper limit for the rate constant for the adduct + Y reaction of 10^{-10} cm^3 molecule^{-1} s^{-1} then the concentration of Y would need to be 10^{15} molecule cm^{-3} to compete with reaction -4a. This is many orders of magnitude greater than the radical concentration in the chamber and we can conclude that reaction 6 is not important in the FTIR chamber. Now consider the different time scales of the experiments. In the pulse radiolysis experiments the kinetic data is derived from monitoring the temporal behavior of the radical species over a time scale of $0-100$ μs. In the FTIR experiments the kinetic data is derived by observing the loss of CH_2BrCl and CH_4 over time scales of 5−15 min. Because reaction −4a occurs on a time scale much less than 5−15 min the FTIR technique will be "blind" to channel 4a and will only provide a measurement of k_{4b}. Hence $k_{4b} = (1.2 \pm 0.4) \times 10^{-11}$ cm^3 molecule^{-1} s^{-1}.

3.8. FTIR Study of the Atmospheric Fate of CHBrClO Radicals. To determine the atmospheric fate of the alkoxy radical CHBrClO formed from reaction 21a, the FTIR−smog chamber system was used to study the products resulting from

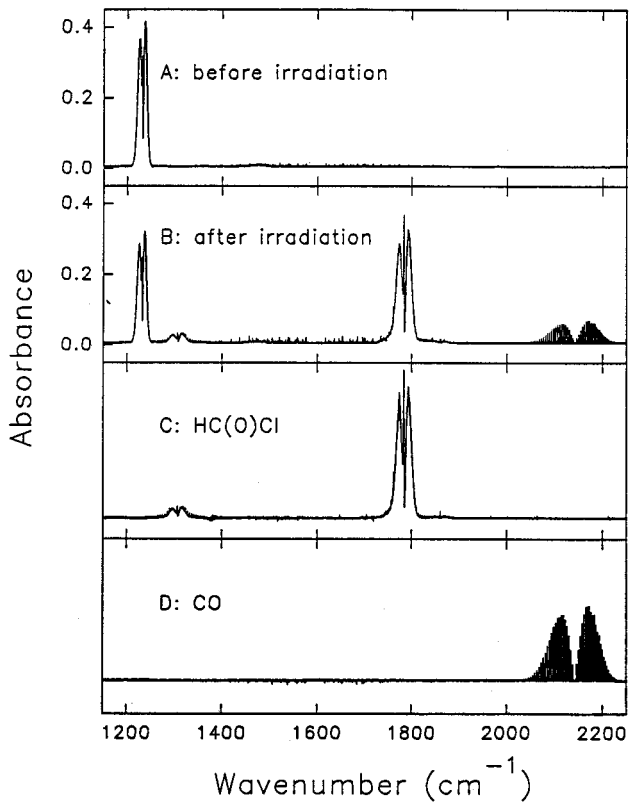

Figure 15. Infrared spectra acquired before (part A) and after (part B) irradiation of a $CH_2BrCl/Cl_2/O_2/N_2$ mixture (see text for details). Parts C and D show reference spectra of HC(O)Cl and CO, respectively.

the Cl atom initiated oxidation of CH_2BrCl with and without NO present. All experiments were performed at 700 Torr total pressure at 295 K. In the absence of NO the CHBrClO alkoxy radical is formed via channel 20a. With NO present it is formed via reaction 21a. The aim of these experiments was to determine

$$CHBrClO_2 + CHBrClO_2 \rightarrow 2CHBrClO + O_2 \quad (20a)$$

$$CHBrClO_2 + CHBrClO_2 \rightarrow CHBrClOH + CBrClO \quad (20b)$$

$$CHBrClO_2 + NO \rightarrow CHBrClO + NO_2 \quad (21a)$$

$$CHBrClO_2 + NO + M \rightarrow CHBrClONO_2 + M \quad (21b)$$

the relative importance of reactions 22−26 in the atmospheric chemistry of CHBrClO radicals.

$$CHBrClO + M \rightarrow HC(O)Cl + Br + M \quad (22)$$

$$CHBrClO + M \rightarrow HC(O)Br + Cl + M \quad (23)$$

$$CHBrClO + M \rightarrow ClCO + HBr + M \quad (24)$$

$$CHBrClO + M \rightarrow BrCO + HCl + M \quad (25)$$

$$CHBrClO + O_2 \rightarrow BrC(O)Cl + HO_2 \quad (26)$$

The loss of CH_2BrCl and the formation of products were monitored using FTIR spectroscopy. Only two carbon containing products were observed: HC(O)Cl and CO. Figure 15 shows FTIR spectra acquired before (part A) and after (part B) a 30 s irradiation of a mixture of 29.9 mTorr of CH_2BrCl, 266 mTorr of Cl_2, and 7 Torr of O_2 in 700 Torr of N_2 diluent. Comparison with the reference spectra of HC(O)Cl and CO given in parts C and D shows the formation of these products.

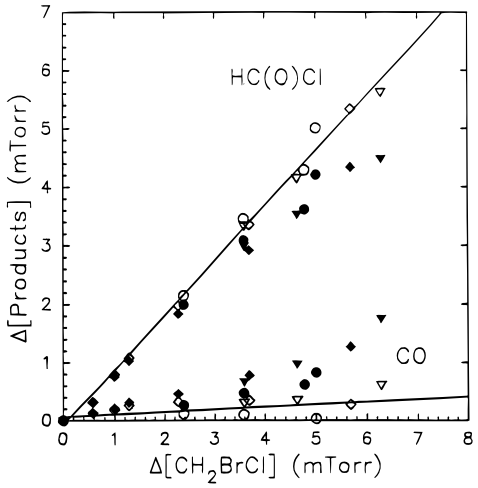

Figure 16. Formation of HC(O)Cl and CO versus CH_2BrCl loss following irradiation of $CH_2BrCl/Cl_2/N_2/O_2$ mixtures at 700 Torr total pressure at 295K. Experimental conditions were 700 Torr of O_2 (circles), 7 Torr O_2 plus 693 Torr of N_2 (triangles), 700 Torr of air with NO added (diamonds). The filled symbols are the observed data; open symbols have been corrected for reaction of Cl atoms with HC(O)Cl. See text for details.

The observed yields of HC(O)Cl and CO are plotted versus the loss of CH_2BrCl in Figure 16.

Careful attention needs to be paid to the possible impact of unwanted secondary reactions which could form or consume the observed products. In addition to reaction with Cl atoms, CH_2BrCl could be lost via photolysis or heterogeneous reactions in the chamber. To test for photolysis, a sample of 17 mTorr of CH_2BrCl in 700 Torr of air was irradiated for 7 min, which is the typical time scale for experiments in this work. To test for heterogeneous loss, a mixture of 32 mTorr of CH_2BrCl and 269 mTorr of Cl_2 in 700 Torr of air diluent was left to stand in the dark for 14 min. In both cases there was no discernible loss (<2%) of CH_2BrCl showing that photolysis and heterogeneous losses of this compound are not significant. The behavior of HC(O)Cl and CO in our reaction chamber have been studied previously.[25] CO is stable in the chamber and reacts slowly with Cl atoms (at 700 Torr, $k(Cl + CO) = 3.2 \times 10^{-14}$ cm^3 molecule^{-1} s^{-1} [18]). There are no significant losses of CO in the chamber. HC(O)Cl undergoes slow heterogeneous decomposition in the chamber with a first-order rate constant of 0.0055 min^{-1};[25] over the experimental time scales used in the present study, heterogeneous loss of HC(O)Cl is negligible. Cl atoms react with HC(O)Cl with a rate constant of $k_{27} = 7.8 \times 10^{-13}$ cm^3 molecule^{-1} s^{-1} [26] (i.e., 1.9 times more rapidly than the reaction of Cl atoms with CH_2BrCl).

$$Cl + HC(O)Cl \rightarrow ClCO + HCl \quad (27)$$

$$ClCO + M \rightarrow Cl + CO + M \quad (28)$$

Corrections for the impact of reaction 27 on the HC(O)Cl and CO product yields were calculated using the expressions

$$[HC(O)Cl]_{corr} = [HC(O)Cl]_{obs}\left(1 - \frac{0.5k_{27}\Delta[CH_2BrCl]}{k_{14}[CH_2BrCl]_0}\right)^{-1}$$

$$[CO]_{corr} = [CO]_{obs} - [HC(O)Cl]_{corr} + [HC(O)Cl]_{obs}$$

where $\Delta[CH_2BrCl]$ is the loss of CH_2BrCl and $[CH_2BrCl]_o$ is the initial concentration. Corrected and uncorrected data are shown in Figure 16. Linear least-squares analysis of the corrected data in Figure 16 give product yields of 94 ± 5%

TABLE 1: Kinetic and Mechanistic Data Determined in This Work for the F + CH_2BrCl Reaction[a]

	section 3.2	section 3.3	section 3.4	section 3.4	section 3.5
k_4 (1000 mbar)		$(4.23 \pm 1.13) \times 10^{-11}$	$(3.6 \pm 1.4) \times 10^{-11}$	$(3.59 \pm 1.12) \times 10^{-11}$	
k_4 (200 mbar)		$(2.15 \pm 1.04) \times 10^{-11}$	$(2.1 \pm 0.9) \times 10^{-11}$	$(1.76 \pm 0.59) \times 10^{-11}$	
K_4	$(4.2 \pm 1.0) \times 10^{-16}$				
Y_X (1000 mbar)		(0.70 ± 0.11)	(0.67 ± 0.30)	(0.67 ± 0.15)	(0.67 ± 0.23)
Y_X (200 mbar)		(0.40 ± 0.28)	(0.43 ± 0.22)	(0.45 ± 0.24)	
$k_{4a,0}$			$(1.78 \pm 0.72) \times 10^{-30}$	$(3.51 \pm 2.07) \times 10^{-30}$	
$k_{4a,\infty}$			$(8.93 \pm 0.63) \times 10^{-11}$	$(7.33 \pm 4.71) \times 10^{-11}$	

[a] Units are cm^3 $molecule^{-1}$ s^{-1} for k_4 and $k_{4a,\infty}$, cm^6 $molecule^{-2}$ s^{-1} for $k_{4a,0}$, and cm^3 $molecule^{-1}$ for K_4

and $4 \pm 6\%$ for HC(O)Cl and CO, respectively. Within the experimental uncertainties we can account for 100% of the CH_2BrCl loss. As seen in Figure 16, variation of the O_2 partial pressure over the range 7−700 Torr and the consumption of CH_2BrCl over the range 4−23% had no discernible impact on the product yields. Furthermore, the presence of NO had no impact on the product yields showing that the yields of HC(O)Cl and CO are independent of the source of CHBrClO radicals (reactions 20a or 21a) and that reaction 21b is not an important channel in the reaction of $CHBrClO_2$ radicals with NO.

As noted above, HC(O)Cl and CO were the only carbon-containing products that were observed, and there was no evidence for any formation of HC(O)Br (<2%) or BrC(O)Cl. From the $4 \pm 6\%$ yield of CO it is possible to conclude that reaction 22 is the only loss mechanism of CHBrClO radicals. Alternatively, the small CO yield may reflect the minor importance of HBr or HCl elimination (reactions 24 and 25) or possibly the formation of BrC(O)Cl followed by some rapid (unknown) process which converts BrC(O)Cl into CO, or all three of these sources of CO could contribute. However, it is clear that the sum of reactions 23−26, if operative, comprise <10% of the fate of the CHBrClO radicals.

The Cl atom initiated oxidation of CH_2BrCl in air at 298 K has been studied previously by Itoh et al.[27] CO and CO_2 were major carbon-containing products, while HC(O)Cl was a minor product. From an analysis of the formation of HC(O)Cl versus loss of CH_2BrCl, Itoh et al.[27] concluded that CHBrClO radicals eliminate both Br and Cl atoms with $k_{22}/(k_{22} + k_{23}) = 0.75$. This conclusion is inconsistent with our observation of essentially quantitative conversion of CH_2BrCl into HC(O)Cl (see Figure 16). The most likely cause of the discrepancy between the two studies is a systematic error in the calibration of the HC(O)Cl yield in the previous work. The conversion of CH_2BrCl into HC(O)Cl illustrated in Figure 16 shows that the fate of CHBrClO radicals in the atmosphere is elimination of Br atoms to form HC(O)Cl. This behavior is analogous to that of CH_2BrO and $CHBr_2O$ radicals which eliminate Br atoms rapidly to form HCHO[28] and HC(O)Br[29], respectively. As discussed previously, a lower limit for the rate of Br atom elimination can be estimated from the absence of the carbonyl product, BrC(O)Cl, expected from reaction 26 as follows. Rate constants for reactions of alkoxy radicals with O_2 lie in the range $(2-60) \times 10^{-15}$ cm^3 $molecule^{-1}$ s^{-1} [18] and appear to be anticorrelated with the C−H bond strength. The C−H bond strength in the CHBrClO radical is likely to be weak and so an estimate of $k_{26} > 10^{-14}$ cm^3 $molecule^{-1}$ s^{-1} seems reasonable. From Figure 16 it can be seen that in the presence of 700 Torr of O_2 the elimination of Br atoms occurs at least an order of magnitude more rapidly that does reaction with O_2. Hence, $k_{22} > 2 \times 10^6$ s^{-1}.

4. Conclusion

Two experimental techniques were used to study the kinetics and mechanism of the reaction of F atoms with CH_2BrCl. The results are given in Table 1 and show that reaction 4 proceeds via two channels:

$$F + CH_2BrCl \rightleftharpoons CH_2BrCl\cdots F \qquad (4a, -4a)$$

$$F + CH_2BrCl \rightarrow CHBrCl + HF \qquad (4b)$$

In 1000 mbar of SF_6 diluent at 296 K, the yield of the $CH_2BrCl\cdots F$ adduct is approximately 70%, while in 200 mbar of SF_6 diluent the yield drops to about 45%. We have recently reported adduct formation in the reactions of F atoms with CH_3Br[6] and CF_2BrH.[5] Bozelli at al.[30] have reported evidence for the formation of an adduct in the reaction of F atoms with CF_3Br. It appears that adduct formation is a general feature of the reaction of F atoms with brominated organic compounds. Throughout this work the adduct has been denoted as $CH_2BrCl\cdots F$ adduct. This "formula" has no implications concerning the structure of the adduct. While the structure of the adduct is unknown, it seems likely that the attacking F atom is bound to the bromine atom in the organic compound. Computational studies are needed to establish the structure of the adduct.

TABLE 2: Comparison of Equilibrium Constants, Adduct Yields, and Absorption Maxima for Adducts Formed between Fluorine Atoms and Brominated Methanes in 1000 mbar of SF_6 at 296 K

reaction	K_{eq} (cm^3 $molecule^{-1}$)	adduct yield (1000 mbar)	absorption maximum (nm)	ref
F + CF_3Br	$<1 \times 10^{-18}$			5
F + CCl_3Br	$<1 \times 10^{-18}$			5
F + CF_2BrH	1.6×10^{-17}	≈100%	295	4
F + CH_2BrCl	4.2×10^{-16}	68 ± 11%	300	this work
F + CH_3Br	$>5 \times 10^{-16}$	31 ± 5%	300	5

Literature data for adduct yields, wavelength of maximum absorption by the adduct, and equilibrium constants for the adduct forming channel in the reaction of F atoms with brominated methanes in the gas phase are given in Table 2. The adduct yield decreases as the number of H atoms in the molecule increases reflecting the increasing importance of H-atom abstraction. The UV absorption spectrum obtained following radiolysis of a mixture of SF_6/CH_2BrCl indicates that the $CH_2BrCl\cdots F$ adduct shows two broad UV absorption bands: a weak feature centered at ≈255 nm and a more intense feature at ≈300 nm as is seen in the UV absorption spectra of the CF_2BrH--F and CH_3Br--F adducts. As noted previously,[6] the equilibrium constant (i.e., the binding energy of the adduct) decreases with the introduction of electronegative substituents. This trend is consistent with electronegative substituents withdrawing electron density from the Br atom thereby reducing the attraction between the Br and the attacking F atom.

Adducts formed from the reaction of halogen atoms with different kinds of electron donors have been observed in solution by pulsed radiolysis and flash photolysis. Examples are iodine atom complexes with benzene, ethyl bromide, and ethyl iodide,[31,32] bromine atom complexes with benzene,[31] and iodine atom complexes with polar solvents.[31,32,33] The lifetimes of

these adducts are of the order of microseconds to milliseconds. Adducts observed in solution have been interpreted as charge transfer (CT) complexes according to the Mulliken theory,[34] and it is established that the charge transfer energy (energy of maximum absorption) increases with increasing ionization potential of the electron donor.[31] As pointed out by Mulliken,[34] structural differences between adducts in solution and in the gas phase influence the thermodynamic properties of the adducts. Chemical and physical knowledge concerning a larger number of gas phase halogen adducts is needed before comparison and general conclusions about structural and thermodynamic properties of gas phase adducts are possible.

Finally, we show here that the atmospheric fate of CHBrClO radicals is elimination of a Br atom which is estimated to proceed with a rate $>2 \times 10^6$ s^{-1} in 700 Torr of air at 296 K.

Appendix

Consider the reaction system:

$$CH_2BrCl + F \rightleftharpoons X \rightarrow P \qquad \text{(a, -a, 6)}$$

$$CH_2BrCl + F \rightarrow CHBrCl + HF \qquad \text{(b)}$$

The time dependence of X and F are given by the differential equations I and II:

$$\frac{d[X]}{dt} = k_a[RH][F] - (k_{-a} + k_6)[X] \qquad \text{(I)}$$

$$\frac{d[F]}{dt} = -(k_a + k_b)[RH][F] + k_{-a}[X] \qquad \text{(II)}$$

where [RH] is the concentration of CH_2BrCl which is assumed to be independent of time. This is a set of coupled first-order linear differential equations which can be reduced to one second-order equation III:

$$\frac{d^2[X]}{dt^2} + ((k_a + k_b)[RH] + k_{-a} + k_6)\frac{d[X]}{dt} + (k_a k_6 + k_b k_{-a} + k_b k_6)[RH][X] = 0 \qquad \text{(III)}$$

This equation can be solved analytically. The roots (m_1, and m_2) of the characteristic equation are:

$$m_1 = \frac{-(k_a + k_b)[RH] - (k_{-a} + k_6) + \sqrt{((k_a + k_b)[RH] + k_{-a} + k_6)^2 - 4(k_a k_6 + k_b k_{-a} + k_b k_6)[RH]}}{2}$$

$$m_2 = \frac{-(k_a + k_b)[RH] - (k_{-a} + k_6) - \sqrt{((k_a + k_b)[RH] + k_{-a} + k_6)^2 - 4(k_a k_6 + k_b k_{-a} + k_b k_6)[RH]}}{2} \qquad \text{(IV)}$$

and the concentration of the adduct as a function of time is given by equation V:

$$[X] = c_1 e^{m_1 t} + c_2 e^{m_2 t} \qquad \text{(V)}$$

At time $t = 0$ the concentration of X is zero, and hence $c_1 = -c_2$ so that [X] as a function of time is given by equation VI

$$[X](t) = c(e^{m_1 t} - e^{m_2 t}) \qquad \text{(VI)}$$

The time where the concentration of X is at its maximum is found by differentiating X with respect to time and equating this with zero:

$$0 = c(m_1 e^{m_1 t_{max}} - m_2 e^{m_2 t_{max}})$$

$$t_{max} = \frac{\ln(m_1/m_2)}{m_2 - m_1} \qquad \text{(VII)}$$

To obtain the maximum concentration of X, t_{max} is inserted into equation VI

$$[X]_{max} = c\left(\left(\frac{m_1}{m_2}\right)^{m_1/(m_2-m_1)} - \left(\frac{m_1}{m_2}\right)^{m_2/(m_2-m_1)}\right) \qquad \text{(VIII)}$$

To find an expression for c, the condition $[F]_0 = [F] + [X] + [R]$ is used:

$$\frac{d[F]}{dt} = -\frac{d[X]}{dt} - \frac{d[R]}{dt} - \frac{d[P]}{dt} \qquad \text{(IX)}$$

By inserting expression VI for [X] and $k_b[RH][F]$ for $d[R]/dt$, and using that $[F] = [F]_0$ at time $t = 0$, expression X for c is obtained:

$$c = \frac{k_a[RH][F]_0}{m_1 - m_2} \qquad \text{(X)}$$

The maximum concentration of adduct as a function of the concentration of RH, k_a, k_{-a}, and k_b is given by

$$[X]_{max} = \frac{k_a[RH][F]_0}{m_1 - m_2}\left(\left(\frac{m_1}{m_2}\right)^{m_1/(m_2-m_1)} - \left(\frac{m_1}{m_2}\right)^{m_2/(m_2-m_1)}\right) \qquad \text{(XI)}$$

Consider the special case where $k_6 = 0$. We define $n_1 = m_1/k_a$, $n_2 = m_2/k_a$, $k = k_{-a}/k_a$, and $\alpha = k_b/k_a$. In terms of these new parameters the maximum concentration of adduct is given as a function of [RH], K, and α through equation XII:

$$[X]_{max} = \frac{[RH][F]_0}{n_1 - n_2}\left(\left(\frac{n_1}{n_2}\right)^{n_1/(n_2-n_1)} - \left(\frac{n_1}{n_2}\right)^{n_2/(n_2-n_1)}\right), \quad \text{for } k_6 = 0 \qquad \text{(XII)}$$

where

$$n_1 = \frac{-(1+\alpha)[RH] - k + \sqrt{((1+\alpha)[RH] + k)^2 - 4k\alpha[RH]}}{2}$$

$$n_2 = \frac{-(1+\alpha)[RH] - k - \sqrt{((1+\alpha)[RH] + k)^2 - 4k\alpha[RH]}}{2} \qquad \text{(XIII)}$$

References and Notes

(1) World Meteorological Organization. Global Ozone Research and Monitoring Project. Report No. 20; Scientific Assessment of Stratospheric Ozone, Appendix; AFEAS Report, 1989; Vol.2, Chapter 6.

(2) Robin, M. L. In *Halon Replacements: Technology and Science*; Miziotek, A. W., Tsang, W., Eds.; ACS Symposium Series 611, American Chemical Society, Washington, DC, 1995; p 85.

(3) Orkin, V. L.; Khamaganov, V. G.; Guschin, A. G.; Huie, R. E.; Kurylo, M. J. *J. Phys. Chem. A* **1997**, *101*, 174.

(4) Atkinson, R. *J. Phys. Chem. Ref. Data* 1989 (Monograph No. 1).

(5) Bilde, M.; Sehested, J; Møgelberg, T. E.; Wallington, T. J.; Nielsen, O. J. *J. Phys. Chem.* **1996**, *100*, 7050.

(6) Sehested, J.; Bilde, M.; Møgelberg, T. E.; Wallington, T. J.; Nielsen, O. J. *J. Phys. Chem.* **1996**, *100*, 10989.
(7) Wine, P. H. Presented at the 210th National ACS Meeting of the American Chemical Society, Chicago, Aug 1995.
(8) Nielsen, O. J. Risø-R-480 (1984).
(9) Wallington, T. J.; Japar, S. M. *J. Atmos. Chem.* **1989**, *9*, 399.
(10) Wallington, T. J.; Dagaut, P.; Kurylo, M. J. *Chem. Rev.* **1992**, *92*, 667.
(11) Bilde, M.; Møgelberg, T. E.; Sehested, J.; Nielsen, O. J.; Wallington, T. J.; Hurley, M.; Japar, S. M.; Dill, M.; V. L. Orkin; Buckley, T. J.; Huie, R. E.; Kurylo, M. J. *J. Phys. Chem. A* **1997**, *101*, 3514.
(12) Wallington, T. J.; Orlando, J. J.; Tyndall, G. S. *J. Phys. Chem.* **1995**, *99*, 9437.
(13) Villenave, E.; Lesclaux, R. *Chem. Phys. Lett.* **1995**, *236*, 376.
(14) Roussel, P. B.; Lightfoot, P. D.; Caralp, F.; Catoire, V.; Lesclaux, R.; Forst, W. *J. Chem. Soc., Faraday Trans.* **1991**, *87*, 2367.
(15) Wallington, T. J.; Hurley, M. D.; Shi, J.; Maricq, M. M.; Sehested, J.; Nielsen, O.J.; Ellermann, T. *Int. J. Chem. Kinet.* **1993**, *25*, 651.
(16) Pershy, A. *J. Phys. Chem.* **1996**, *100*, 689.
(17) Troe, J. *J. Phys. Chem.* **1979**, *83*, 114.
(18) DeMore, W. B.; Sander, S. P.; Golden, D. M., Hampson, R. F.; Kurylo, M. J.; Howard, C. J.; Ravishankara, A. R.; Kolb, C. E.; Molina, M. J. Technical Publication 94-26; Jet Propulsion Laboratory: Pasadena, CA, 1994.
(19) Burley, J. D.; Miller, C. E.; Johnston, H. S. *J. Mol. Spectrosc.* **1993**, *158*, 377.
(20) Sehested, J.; Ellermann, T.; Nielsen, O. J.; Wallington, T. J. *Int. J. Chem. Kinet.* **1994**, *26*, 615.
(21) Wallington, T. J.; Ellermann, T.; Nielsen, O. J.; Sehested, J. *J. Phys. Chem.* **1994**, *98*, 2346.
(22) Wallington, T. J.; Hurley, M. D. *Chem. Phys. Lett.* **1992**, *189*, 437.
(23) Tschuikow-Roux; E., Faraji, F.; Paddison, S.; Niedzielski, J.; Miyokawa, K. *J. Phys. Chem.* **1998**, *92*, 1488.
(24) Wallington, T. J.; Hurley, M. D. *Chem. Phys. Lett.* **1992**, *193*, 84.
(25) Kaiser, E. W.; Wallington, T. J. *J. Phys. Chem.* **1994**, *98*, 5679.
(26) Niki, H.; Maker, P. D.; Savage, C. M.; Breitenbach, L. P. *Int. J. Chem. Kinet.* **1980**, *12*, 1001.
(27) Ioth, K.; Kato, J.; Nakayama; Kutsuna, S.; Koike, K.; Ibusuki, T. *Chemosphere* **1994**, *29*, 1701.
(28) Orlando, J. J.; Tyndall, G. S.; Wallington, T. J. *J. Phys. Chem.* **1996**, *100*, 7026.
(29) Orlando, J. J.; Tyndall, G. S., Wallington, T. J.; Dill, M. *Int. J. Chem. Kinet.* **1996**, *28*, 433.
(30) Bozzelli, J. W.; Kolb, C. E.; Kaufman, M. *J. Chem. Phys.* **1973**, *59*, 3669.
(31) Bühler, R. E. *J. Phys. Chem.* **1972**, *76*, 3220.
(32) Gover, T. A.; Porter, G. *Proc. Roy. Soc. London, Ser. A* **1961**, *261*, 475.
(33) Fornier de Violet, P.; Bonneau, R.; Joussot-Dubien, J. *Chem. Phys. Lett.* **1973**, *19*, 251.
(34) Mulliken, R. S.; Person, W. B. Molecular Complexes, A lecture and Reprint Volume; Wiley & Sons: New York, 1969.